Journal of Power Sources 235 (2013) 135–141

Contents lists available at SciVerse ScienceDirect

Journal of Power Sources

journal homepage: www.elsevier.com/locate/jpowsour

Short communication

Preparation of high-performance PdPt–Pt core–shell catalyst with shortened carbon nanotubes as support

Yan-Ni Wu [a,*], Shi-Jun Liao [b], Hai-Fu Guo [a], Xiang-Ying Hao [a]

[a] School of Chemistry and Chemical Engineering, Zhao Qing University, Zhao Qing 526061, China
[b] School of Chemistry and Chemical Engineering, South China University of Technology, Guangzhou 510641, China

HIGHLIGHTS

- Shortened carbon nanotubes are used as supports for core–shell PdPt@Pt/SCNTs catalyst.
- The mass activity for PdPt@Pt/SCNTs catalyst is 2.87 times higher than JM 40 wt% Pt/C catalyst.
- The catalyst shows better poisoning tolerance than PtRu/C catalyst.
- The enhanced activity observed did not alter the ORR pathway.

GRAPHICAL ABSTRACT

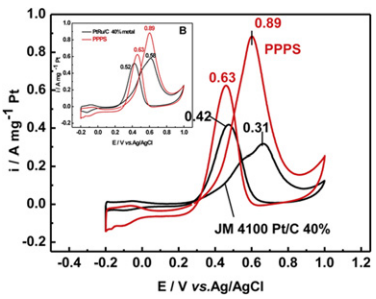

ARTICLE INFO

Article history:
Received 2 December 2012
Received in revised form
24 January 2013
Accepted 5 February 2013
Available online 16 February 2013

Keywords:
Core–shell catalyst
Low-Pt catalyst
Methanol anodic oxidation
Oxygen reduction reaction
Shortened carbon nanotubes

ABSTRACT

Shortened carbon nanotubes (SCNTs) obtained by ball milling of carbon nanotubes (5–10 μm) with the assistance of ethanol are used as supports for fabrication of core–shell structured PdPt@Pt/SCNTs via a successive colloidal reduction approach. The catalysts are characterized by X-ray diffraction (XRD) analysis, Transmission electron microscopy, and X-ray photoelectron spectroscopy. The active particles are found to disperse on the shortened carbon nanotubes with an average particle size of 3.1 nm. PtPd nanoparticles, rather than single Pd nanoparticles, are used as core materials for prevention of possible agglomeration and better dispersion. Using this catalyst, we investigate methanol oxidation reactions (MOR) and oxygen reduction reactions (ORR). The catalysts show excellent activity to anodic MOR, 2.87 times higher than that of commercial Johnson Matthey 40 wt.% Pt/C catalyst. The ratio of forward current I_f to backward current I_b is as high as 1.41 for the oxidation of methanol relative to that of 0.74 for the commercial Pt/C catalyst, an indication of better CO tolerance of the former. In the ORR, the reaction is found to proceed via an overall four-electron transfer process.

1. Introduction

Platinum is the best catalyst for both anode and cathode of proton exchange membrane fuel cell (PEMFC). The high cost of the precious metal Pt and easy poisoning of Pt-based catalysts by carbon monoxide (CO) hinder the commercialization of direct methanol fuel cells (DMFCs) [1]. Two major approaches have been adopted to improve the electrochemical catalyst performance: decreasing the loading of Pt in the catalyst by utilizing a new structure and increasing the utilization efficiency of Pt through new kinds of support materials.

To reduce Pt loading, significant research efforts have been made to develop techniques for designing low-Pt [2,3] and core–shell-structured [4–6] catalysts because of their unique physiochemical properties. Among studies on low-Pt catalysts, the core–shell construction of nanosized bimetallic particles provides the

* Corresponding author. Tel.: +86 0758 2716357.
E-mail address: yanniwu@163.com (Y.-N. Wu).

0378-7753/$ – see front matter © 2013 Elsevier B.V. All rights reserved.
http://dx.doi.org/10.1016/j.jpowsour.2013.02.011

possibility of increasing the utilization of the catalyst, thus lowering catalyst loading. Adzic et al. synthesized and characterized Pt monolayer core–shell electrocatalysts with noble metals (e.g., Au [7,8], Pd [8], doped-metal Pt [9]), and core–shells formed by non-noble metals and noble metals [10], among others, by utilizing the underpotential deposition method with excellent results. Core–shell catalysts with minimal Pt contents show very high activity for oxygen reduction compared with pure Pt oxygen reduction reaction (ORR) catalysts. However, the prepared catalysts are in the form of bulk particles, which significantly decreases the utilization efficiency of Pt.

Inspired by the idea that Pt monolayers deposited on suitable substrates show higher activity than those deposited on bulk metal surfaces, we designed experiments to replace core Pt metal atoms with other less-expensive metals (e.g., Pd). While palladium is much cheaper than platinum and has better tolerance to the chemical corrosion and electrochemical corrosion, we used Pt–Pd alloy particle as the core instead of pure Pd nanoparticle to obtain high dispersion and prevent possible agglomeration. This approach allows significant reductions in the use of the shell metal Pt so that high surface-to-volume ratios of Pt can be obtained. Since our experiments show that as support shortened carbon nanotubes (SCNTs) have considerable advantages over normal carbon nanotubes [11], including high dispersion of active components, high performance resulted from high surface area, and the easy dispersion of the catalyst in the solvent for the preparation of membrane electrode assembly (MEAs), we prepared a core–shell catalyst with such a support. We report here a catalyst consisting of a Pt–Pd core covered with a shell of Pt atoms with SCNTs as support (PtPd@Pt/SCNTs).

Another major approach in enhancing the utilization efficiency of precious metal electrocatalysts to increase the electrochemically active surface area of the catalyst is exploration of the surface area of carbon supports [12,13], such as carbon, carbon nanotubes (CNTs) [14], and carbon nanofibers [15], among others. Antolini [16] discussed novel non-conventional carbon materials used as supports from ordered mesoporous carbons, carbon aerogels, carbon nanotubes, carbon nanohorns, carbon nanocoils, and carbon nanofibers. Because of their unique structure, large surface area, low resistance, and high stability in electrochemistry, CNTs have been widely used as catalyst supports [17,18]. However, their length and the easy-to-tangle features make it difficult to prepare membrane electrode assembly. To ameliorate this problem, alternative supporting carbon materials, such as shorted CNTs (SCNTs), may be explored. Recently, Wang, et al. [19] reported the use of an Fe compound (FeS) as a catalyst for controlling the length of CNTs (<300 nm). CNTs have also been used as a catalyst support for proton exchange membrane fuel cells; in this application, short CNTs were found to show much better performance than conventional long CNTs. The result is consistent with our previous report [20].

In this study, the PdPt@Pt/SCNTs (denoted as PPPS hereafter) catalyst was prepared with a core–shell structure. SCNTs of approximately 200 nm were obtained by the ball milling method using ethanol as the milling aid agent. This material was used as a support in a facile two-stage colloidal approach to improve the CO tolerance and methanol electro-oxidation activity of the resulting catalyst, as well as reduce its cost. The electrochemical performance results of the PPPS catalyst in methanol anodic oxidation show its high electrocatalytic activity and superior ability to resist CO-poisoning in acidic medium for DMFCs. Given the excellent performance of our catalyst in MOR, we are also interested to investigate the role of the PPPS core–shell structure in ORR. Inasmuch as Pt catalyst prefers an overall four-electron transfer reaction while Pd catalyst prefers overall two-electron transfer reaction, it is interesting to explore the ORR mechanism when using the PPPS core–shell structures. Using PPPS, we find that the kinetic mechanism of ORR involves a favorable overall four-electron transfer reaction.

2. Experimental

2.1. Pretreatments and ball milling of carbon nanotubes

Multi-walled CNTs with an average diameter of ca. 20 nm and average lengths of ca. 5 μm–15 μm were obtained from Tsinghua University, China. The CNTs were shortened by the ball milling method with a milling machine (QM-3SP04 Planet Type Milling Machine, NanJing University Instrument Plant, China) for 120 h using ethanol as a milling aid agent. To yield the support, SCNTs were oxidized in a mixture of 5% H_2O_2 + 10% HNO_3 solution under reflux at 80 °C for 3 h, followed by extensive washing with deionized water and air drying at 70 °C overnight.

2.2. Preparation of PPPS electrocatalyst

SCNTs-supported Pd–Pt alloy cores (PdPt/SCNTs) were prepared by an organic colloid method [21]. Palladium chloride and sodium citrate were dissolved in ethylene glycol (EG) and stirred for 30 min. Hexachloroplatinate acid and sodium citrate were then added to the solution and stirring continued for another 30 min. The sodium citrate was used as a complexing agent and stabilizer, which lead to smaller nanoparticles and better dispersion. SCNTs were added to the mixture (metal loading of Pd- and Pt-cores of 12 wt.% and 3 wt.%, respectively) with stirring. The pH of the solution was adjusted to >10 by the drop-wise addition of a 5 wt.% KOH/EG solution with vigorous stirring. The mixture was then placed into a Teflon-lined autoclave and conditioned at 160 °C for 8 h, followed by filtering, washing, and vacuum drying at 90 °C. The PPPS catalyst was prepared by depositing a shell Pt layer on the surface of the PdPt/SCNTs prepared in last step (metal loading of Pt-shell of 5 wt.%). The method and procedures were similar to PdPt/SCNTs approach, except that no palladium chloride was added to the solution. The total metal loading was ca. 20 wt.% and the nominal Pt content was ca. 8 wt.%. For comparison, 20 wt.% Pd/C, Pt/C, Pt/SCNTs, PtPd/C, and PPPS catalysts were prepared using the same approach. Both Pt–Pd/C and PPPS catalysts had the same Pt:Pd atom ratio (Pt:Pd = 1:3).

2.3. Electrochemical evaluations

The electrochemical performance of the catalyst was determined by cyclic voltammetry (CV) using a three-electrode cell in an IM6e electrochemical workstation (Zahner, Germany) at room temperature. A Pt wire and an Ag/AgCl electrode were used as the counter and reference electrodes, respectively. The working electrode used was a glassy carbon disk (5 mm in diameter) covered with a thin layer of Nafion-impregnated catalyst. The thin-film electrode was prepared as follows: 5 mg of catalyst was dispersed in 1 mL of Nafion/ethanol (0.25% Nafion) by sonication for 20 min. A CV test was conducted at 50 mV s^{-1} in a solution of 0.5 M H_2SO_4 or 0.5 M H_2SO_4 with 0.5 M CH_3OH and a potential range from −0.2 V to 1.0 V. Four microliters of the dispersion was transferred onto the glassy carbon disk using a pipet. The Pt loadings of the 40% Pt/C and PPPS catalysts on the electrode surface were 0.0080 and 0.0016 mg, respectively. The apparent surface area of the electrode was 0.196 cm^2.

2.4. Material characterization

The morphology of the PPPS catalyst was observed using a scanning transmission electron microscope (STEM, Hitachi 2000

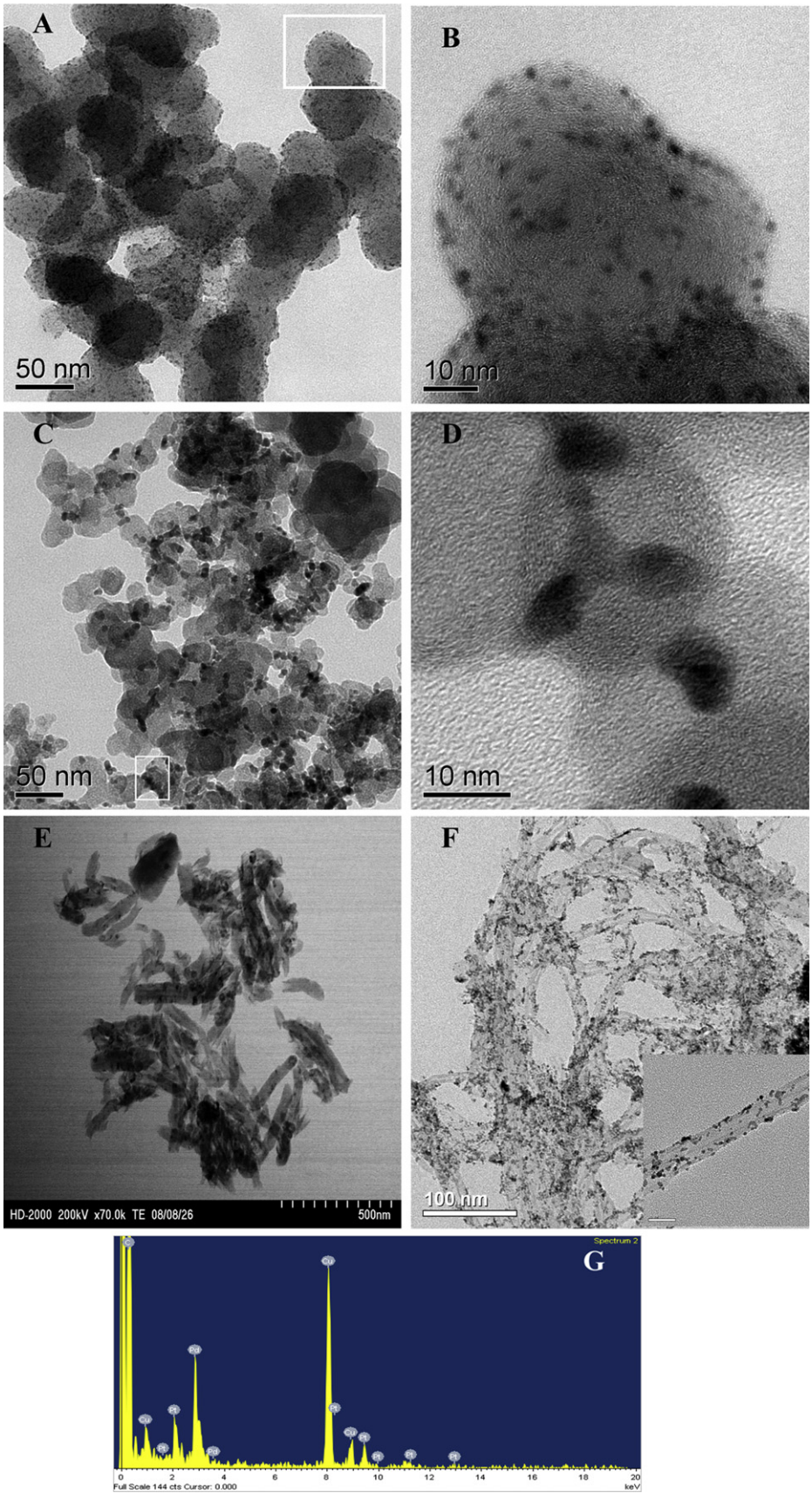

Fig. 1. TEM images of the as-prepared 20 wt.% Pt/C (A and B), Pd/C (C and D), S-CNTs (E), PPPS (F) catalyst, and the energy-dispersive X-ray analysis of PPPS(G).

STEM) operating at 200 kV. X-ray diffraction (XRD) analysis was performed using a Shimadzu XD-3A X-ray diffractometer (Japan) with a filtered Cu-Kα radiation source. The tube voltage was maintained at 35 kV and the tube current was 30 mA. Diffraction patterns were collected from 20° to 80° at a scanning rate of 4° min^{-1} and a step size of 0.01°. The surface composition of the catalysts was analyzed by X-ray photoelectron spectroscopy (XPS) using a Perkin Elmer model PHI1600 system with a single Mg Kα X-ray source operating at 300 W and a voltage of 15 kV.

3. Results and discussion

3.1. Catalyst morphology

In Fig. 1A, C, and F, Pt particles are highly dispersed on the different carbon supports with narrow size distribution. The as-prepared 20 wt.% Pt/C (A and B), Pd/C (C and D), and PPPS (F) catalyst nanoparticles are well dispersed with average particle sizes of ca. 2.4 nm, 4.3 nm, and 3.1 nm, respectively. Fig. 1E shows that the nanotubes have been effectively shortened by the ethanol-aided ball milling method, yielding average lengths of ca. 200 nm. The core–shell structure is difficult to observe by STEM because the diameter of the particles is between 2 nm and 5 nm. Indirect evidence of the selective deposition of Pt-shells on the Pd–Pt-core surface was revealed in a previous report [21]. The composition of the PPPS electrocatalyst was determined by energy-dispersive X-ray (EDX) analysis (Fig. 1G). The EDX composition of the prepared catalyst was found to be close to the nominal value.

3.2. Physical characterization

XPS is an ideal technique that allows identification of surface or near-surface species involved in fuel cell catalysis [22]. The chemical composition of PdPt@Pt and Pt nanoparticles deposited onto functionalized SCNTs and carbon was analyzed by XPS. In Fig. 2A and B, the surface Pt–Pd atom ratio of PPPS (0.66) is 3.9 times higher than that of PtPd/C (0.19), indicating that the surface of the PPPS catalyst is rich in Pt. These findings indirectly support the suggestion that the PPPS catalyst has a core–shell structure. The atom percentage of Pt in the PPPS catalyst (0.86%) detected by the XPS fitting curve agrees with the calculation value (0.96%).

The Pt 4f signal of the PPPS catalyst (Fig. 2C) can be deconvoluted into two doublets. Peaks with binding energies of 71.03 eV and 74.45 eV are ascribed to metallic Pt. Peaks corresponding to 71.90 eV and 74.97 eV can be assigned to Pt(II) species in the form of $Pt(OH)_2$ or PtO [23]. In Fig. 2D, the Pt binding energies of the PPPS catalyst are positively shifted compared with those of the Pt/SCNT catalyst, indicating an interaction between Pt in the shell and Pd in the PtPd-core, although a Pt–Pd interaction within the core cannot be excluded.

The Pd 3d levels of PPPS in Fig. 2E only show metallic Pd peaks; no peaks for palladium oxide are observed. In terms of the binding energy of Pd_{3d}, the binding energies of Pd in the core of the PPPS catalyst are lower than those of Pd in the pure Pd/C catalyst (Fig. 2F), which is in contrast to observations of Pt. The negative shift of Pd_{3d} in the core may result from the interaction between Pd and Pt in the alloy.

Fig. 3 shows the XRD patterns of the as-prepared 20 wt.% Pt/C, Pd/C, and PPPS catalysts. The peak distribution indicates the presence of a face-centered cubic (FCC) structure. The first diffraction peak located at about 24.8° in all of the XRD patterns is associated with the (001) diffraction of 20 wt.% Pt/C and Pd/C catalysts, which use Vulcan XC-72 carbon as a support. The diffraction peak of the PPPS catalyst at 24.8° is associated with the (002) diffraction of the hexagonal graphite structure in the carbon materials. The intensity of the peak of the SCNTs sample is much higher than that of the

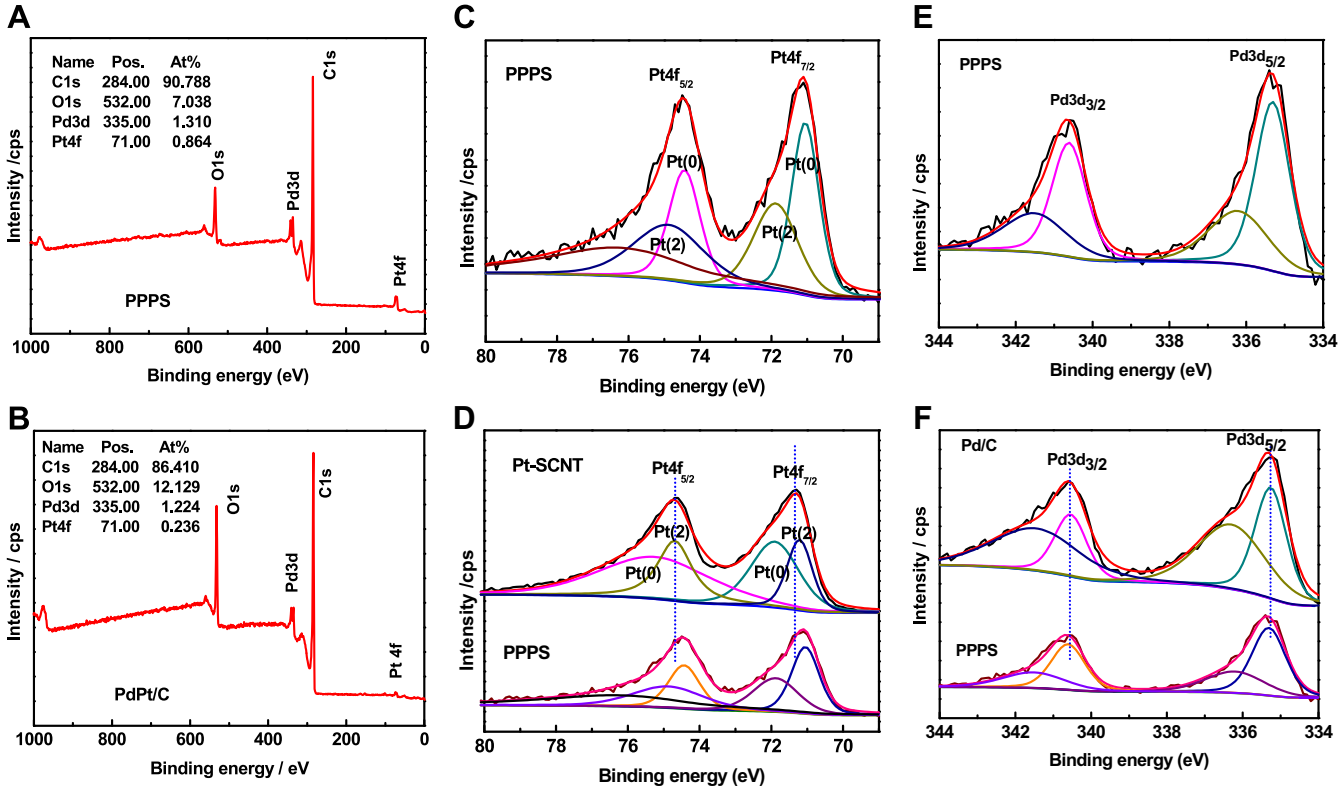

Fig. 2. XPS survey spectrum of PPPS (A) and PtPd/C catalysts (B), the Pt_{4f}XPS spectra of PPPS (C), Pt_{4f}XPS spectrum for 20%Pt/SCNTs and PPPS as a standard (D), Pd_{3d}XPS spectra of PPPS (E), and Pd_{3d}XPS spectra for 20%Pd/C and PPPS as a standard (F).

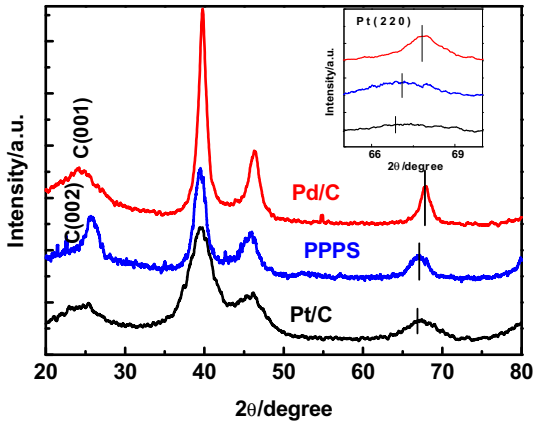

Fig. 3. XRD patterns for the as-prepared 20 wt. % Pt/C, Pd/C and PPPS catalyst.

Vulcan XC-72 carbon sample, indicating the much higher graphitization degree or graphitic crystallinity of SCNTs. A higher degree of graphitization is an important quality of supporting carbon materials to electrocatalysts due to their higher electron conductivity and stronger electronic interaction with the loaded catalytic metal particles [24]. Interestingly, the (220) diffraction peak of PPPS catalyst is between that of Pt/C and Pd/C and is more similar to Pt/C than the Pd/C catalyst. The (220) diffraction peak of the PPPS catalyst shows a negative shift compared with the Pd/C catalyst, suggesting an increase in the lattice constant due to the incorporation of Pt atoms into the Pd crystalline lattice.

The calculated values of the XRD lattice parameters are shown in Table 1. The mean particle size was calculated from the (220) diffraction plane using Jade 5 software, and the XRD results were combined with the TEM findings. The lattice parameters of PPPS catalysts are larger than those of pure Pd but smaller than those of Pt/C.

3.3. The activity of PPPS for anodic methanol oxidation and oxygen reduction

CV is a surface-sensitive technique that detects the electrochemical properties of surface atoms rather than bulk atoms [25]. Fig. 4 shows the base cyclic voltammograms of commercial 40 wt.% Pt/C (Johnson Matthey 4100), Pd/C, and PPPS catalysts in 0.5 M H_2SO_4 under a N_2 atmosphere at room temperature. Several interesting points may be observed. First, the CV curve of the Pd/C catalyst shows large peaks at the potential range from −0.2 V

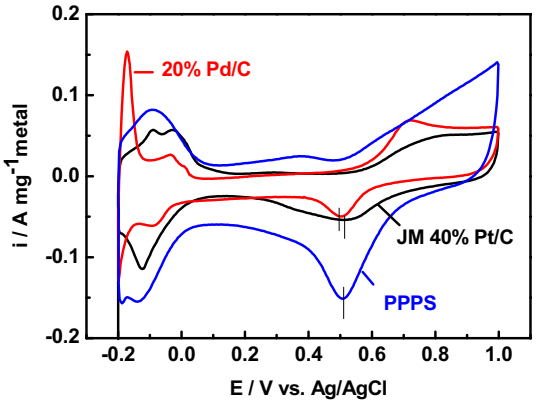

Fig. 4. Cyclic voltammograms of the commercial 40 wt.% Pt/C (Johnson Matthey 4100), 20 wt.% Pd/C and PPPS catalyst measured in N_2-purged 0.5 M H_2SO_4 electrolyte at room temperature and at a sweep rate of 50 mV s^{-1}.

Table 1
Lattice parameters of the 20 wt.% Pt/C, Pd/C and PPPS catalysts.

Sample 20 wt.% metal	XRD crystallite size (nm)[a]	Pt (wt.%)	M–M bond distance (nm)	Lattice parameter (nm)
Pt/C	2.1	20	0.2780	0.3931
Pd/C	4.5	0	0.2756	0.3898
PPPS	3.5	8	0.2778	0.3917

[a] Particle size is estimated from XRD patterns.

to −0.1 V vs. Ag/AgCl, which generally corresponds to the hydrogen adsorption/desorption process; Pt/C and PPPS do not exhibit similar peaks. The surprisingly large peaks could be attributed to the dissolution of adsorbed hydrogen into the bulk Pd. Second, the hydrogen oxidation peak of the PPPS catalyst is smaller to that for pure Pt and the oxide reduction peaks for the Pd/C catalyst are about 0.50 V, whereas those for the Pt/C and PPPS catalysts are about 0.52 V. This result indicates that the Pd core is mainly covered by the Pt shell in the PPPS catalysts. Third, the absence of Pd features and two or three typically resolved peaks in the hydrogen adsorption–desorption region of Pt implies that all or most of the Pt–Pd core surfaces are covered by Pt shells.

CV was performed to measure the electrochemical activity of the methanol oxidation with different catalysts. Fig. 5A shows the cyclic voltammograms of the 40 wt.% Pt/C (JM4100) and PPPS catalysts in 0.5 M CH_3OH + 0.5 M H_2SO_4 solution. The PPPS catalyst shows superior catalytic activity compared with the Pt/C and PtRu/C catalysts. The electrocatalytic mass activity of the PPPS catalyst is evidently much larger than that of the Pt/C catalyst. The current

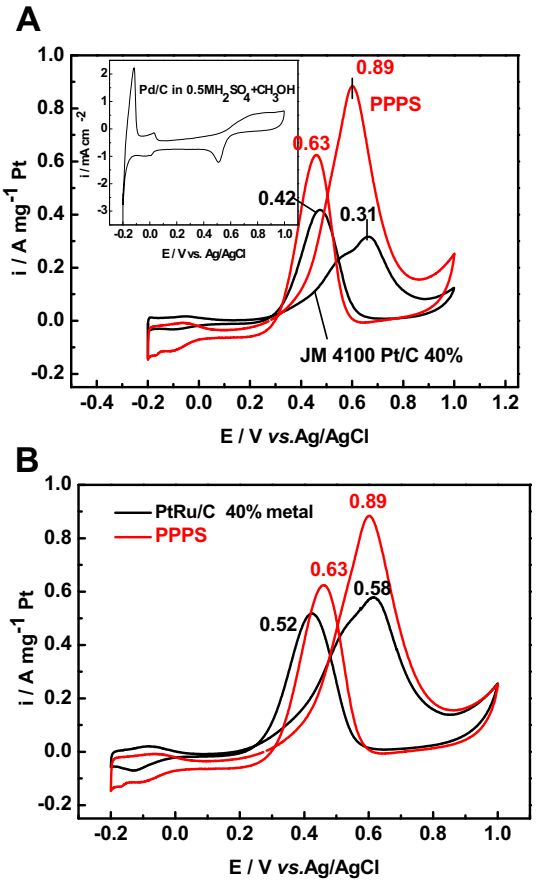

Fig. 5. A: Cyclic voltammograms of the commercial 40 wt.% Pt/C (Johnson Matthey 4100) and PPPS (RDE at 300 rpm) measured in 0.5 M H_2SO_4 + 0.5 M CH_3OH electrolyte at room temperature and at a sweep rate of 50 mV s^{-1}. B: Cyclic voltammograms of the PPPS and 40 wt. % PtRu/C electrode measure as same conditions.

peak near 0.7 V in the forward scan is attributed to methanol electrooxidation. The mass activity value of the PPPS catalyst for methanol electrooxidation is 0.89 A mg^{-1} Pt, which is about 2.87 times larger than that of the Pt/C (JM4100) catalyst.

The CV curve of 20 wt.% Pd/C in 0.5 M CH_3OH + 0.5 M H_2SO_4 solution is included in Fig. 5A. Comparing the CV curves of Pd/C with those of the Pt/C (JM4100) and PPPS catalysts, the PPPS catalyst has the a curve shape similar to that of the pure Pt/C catalyst, indicating that no Pd is present on the surface of the Pt shell. The potential for methanol oxidation in the forward scan of the PPPS catalyst is 0.60 V, much lower than that of the commercial JM catalyst Pt/C (0.66 V). This difference indicates that the PPPS catalyst yields a significantly reduced overpotential during methanol oxidation.

The electrocatalytic mass activity of the PPPS catalyst is 1.5 times larger than that of the 40 wt.% PtRu/C catalyst (Fig. 5B). The superior performance of the PPPS catalyst can be attributed to the interaction between the outer Pt and inner Pd, as well as the high dispersion of the prepared SCNTs. The uniform deposition of PdPt@Pt nanoparticles on the surface of SCNTs improves the deposition of catalyst particles on the electrode [26].

The ratios of peak currents of the catalysts associated with the anodic peaks in the forward (I_f) and reverse (I_b) scans were compared to determine catalyst performance. A larger I_f/I_b value is generally considered as indicative of improved CO tolerance although there are other viewpoints differing with whether PtO or CO-poisoning being playing a role [27–29]. From our experiment, the I_f/I_b of the PPPS catalyst (1.41) is higher than that of the JM Pt/C (0.74) and 40 wt.% PtRu/C (1.12) catalysts. These results indicate that most of the intermediate carbonaceous species on the PPPS catalyst are oxidized to CO_2in the forward scan, resulting in its high tolerance to CO. The high activity and CO tolerance performance of the catalyst may be attributed to the high utilization efficiency of Pt, the underlying Pd and Pt-shell structures, and the shorted CNTs. These structures help significantly improve the oxidative removal of CO_{ads} on the Pt shell by making available several active oxygen-containing species (e.g., PdO/PdO_x) on the underlying Pd core [30].

Fig. 6 shows rotating-disk polarization curves for the ORR of 20 wt.% Pt/C, Pd/C, and PPPS catalysts in an oxygen-saturated 0.5 M H_2SO_4 solution under ambient conditions. The PPPS electrocatalyst shows a current density higher than that of the pure Pd/C catalyst and very similar to that of the 20 wt.% Pt/C catalyst at certain voltage range. The half-wave potentials of PPPS and 20 wt.% Pt/C are 0.50 mV and 0.55 mV, respectively.

To obtain kinetic information on the ORR process, data for the Koutecky–Levich plots were obtained for the reduction of the different catalyst electrodes in an oxygen-saturated 0.5 M H_2SO_4 solution and the results are shown in Fig. 7A and B. Typical linear polarization curves of the ORR of PPPS and as-prepared 20 wt.% Pt/C catalysts at different rotation rates (sweep rate of 5 mV s^{-1}) were inserted into the related Koutecky–Levich plots. We find that the PPPS and Pt/C catalysts exhibit similar trend. The number of electrons exchanged in the reduction of an oxygen molecule could be obtained by the slopes of the Koutecky–Levich plots [26,31]. According to the Koutecky–Levich equation [32,33], this type of graph gives parallel straight lines at different potentials, with a slope equal

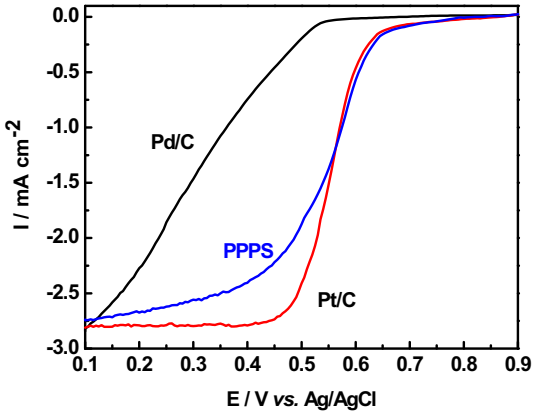

Fig. 6. Polarization curves of 20 wt.% Pt/C, 20 wt.% Pd/C and PPPS catalyst measured in 0.5 M H_2SO_4 solution saturated with pure oxygen, at a scan rate of 5 mV s^{-1} and a rotation speed of 1600 rpm.

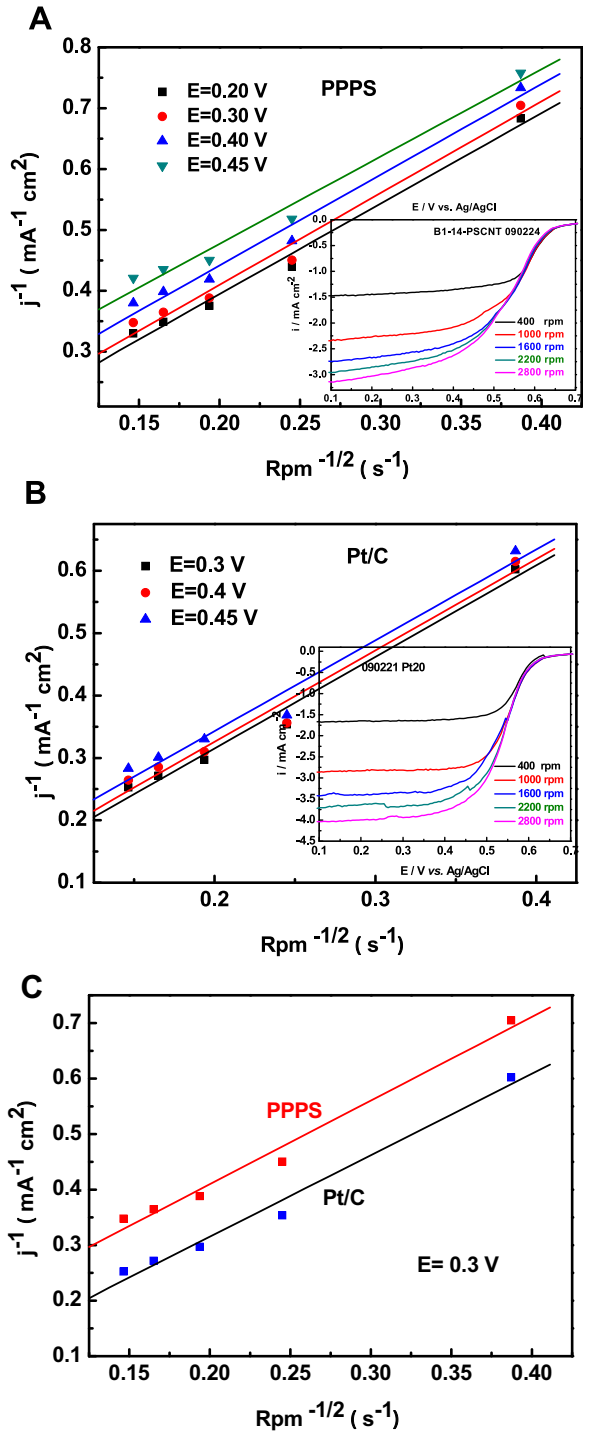

Fig. 7. A, B: Typical Koutecky–Levich plots of catalysts PPPS and 20 wt. % Pt/C prepared from data insert in Fig. 6A, B at different electrode potentials. C: Typical Koutecky–Levich plots of catalysts PPPS and 20 wt. % Pt/C at 0.3 V.

to B^{-1}, where $B = 0.62nFCD^{2/3}\upsilon^{-1/6}$. Here n is the number of electrons transferred per oxygen molecule, F is the Faraday constant (96486.7 C mol^{-1}), Cis the bulk concentration of dioxygen dissolved in the solution (1.5×10^{-6} mol cm^{-3}), D is the diffusion coefficient of oxygen in the solution (1.9×10^{-5} cm s^{-1}), and υ is the kinematic viscosity of the solution (0.01 cm s^{-1}) [34]. The values of n can be calculated from the slopes of the Koutecky–Levich lines in Fig. 7A and B using the indicated parameters. The experimental values of B derived from Fig. 7A and B are highly similar at 0.6052 mA cm^{-2} $s^{-1/2}$and 0.6056 mA cm^{-2} $s^{-1/2}$, respectively (Fig. 7C). The calculated n values are very close to 4, suggesting that both ORRs with the PPPS and Pt/C catalysts could proceed via an overall four-electron transfer reaction to form water directly, i.e., $O_2 + 4H^+ + 4e \rightarrow 2H_2O$.In other words, our PdPt@Pt/SCNTs catalyst acts as a Pt catalyst rather than a Pd catalyst toward the oxygen reduction reaction, further verifying the core–shell structure of the catalyst.

4. Conclusions

We have prepared in a facile two-stage colloid route an ultra-low Pt-containing core–shell catalyst PdPt@Pt/SCNTs with SCNTs as a support for methanol oxidation reactions and oxygen reduction reactions. This electrocatalyst is found to possess excellent electrocatalytic properties for methanol anodic oxidation and superior CO tolerance when Pt loading is significantly reduced to as low as 1/5 of the JM 40% Pt/C catalyst. The enhanced activity of the proposed catalyst for methanol oxidation may be attributed to the larger surface area of SCNTs compared with normal carbon and synergetic catalytic effects between the Pt–Pd-core and Pt-shell. In addition, the PdPt@Pt/SCNTs catalyst has comparable performance with 20% wt. Pt/C catalyst in oxygen reduction reaction. It is found that the core–shell structure does not alter the 4-electron transfer pathway. Given this core–shell structure possess higher Pt utilization efficiency, our catalyst provides an opportunity for reducing the cost of direct methanol fuel cells while maintaining comparable reaction pathway. Further investigations on the electrocatalytic performance of PdPt@Pt nanoparticles supported on CNTs with different lengths is interesting.

Acknowledgments

This work is financially supported by National Scientific Foundation of China (NSFC Project Nos. 20673040, 20876062), the Guangdong Provincial Scientific Foundation (Project No. 36055 , S2012040007383), and the Key Laboratory of Fuel Cell Technology of Guangdong Province.

References

[1] G. Pérez, E. Pastor, C.F. Zinola, Int. J. Hydrogen Energy 34 (2009) 9523–9530.
[2] S.A. Francis, S.H. Bergens, J. Power Sources 196 (2011) 7470–7480.
[3] Y. Ando, K. Sasaki, R. Adzic, Electrochem. Commun. 11 (2009) 1135–1138.
[4] J. Zhang, X. Zhang, M. Tu, W. Liu, H. Liu, J. Qiu, L. Zhou, Z. Shao, H.L. Ho, K.L. Yeung, J. Power Sources 198 (2012) 14–22.
[5] L. Zhang, J. Kim, H.M. Chen, F. Nan, K. Dudeck, R.S. Liu, G.A. Botton, J. Zhang, J. Power Sources 196 (2011) 9117–9123.
[6] H. Naohara, Y. Okamoto, N. Toshima, J. Power Sources 196 (2011) 7510–7513.
[7] J. Zhang, K. Sasaki, E. Sutter, R. Adzic, Science 315 (2007) 220–222.
[8] J. Zhang, Y. Mo, M.B. Vukmirovic, R. Klie, K. Sasaki, R.R. Adzic, J. Phys. Chem. B 108 (2004) 10955–10964.
[9] J. Zhang, M.B. Vukmirovic, K. Sasaki, A.U. Nilekar, M. Mavrikakis, R.R. Adzic, J. Am. Chem. Soc. 127 (2005) 12480–12481.
[10] M. Shao, K. Sasaki, N.S. Marinkovic, L. Zhang, R.R. Adzic, Electrochem. Commun. 9 (2007) 2848–2853.
[11] Y.N. Wu, S.J. Liao, H.N. Su, D. Dang, B. Liu, Fuel Cells 10 (2010) 920–925.
[12] B. Fang, J.H. Kim, M. Kim, J.S. Yu, Chem. Mater. 21 (2009) 789–796.
[13] W. Li, X. Wang, Z. Chen, M. Waje, Y. Yan, Langmuir 21 (2005) 9386–9389.
[14] M.O. Danilov, A.V. Melezhyk, J. Power Sources 163 (2006) 376–381.
[15] B.K. Balan, S.M. Unni, S. Kurungot, J. Phys. Chem. C 113 (2009) 17572–17578.
[16] E. Antolini, Appl. Catal. B 88 (2009) 1–24.
[17] Y. Zhao, X. Yang, J. Tian, F. Wang, L. Zhan, Int. J. Hydrogen Energy 35 (2010) 3249–3257.
[18] S. Wang, S.P. Jiang, T.J. White, X. Wang, Electrochim. Acta 55 (2010) 7652–7658.
[19] X. Wang, J. Wang, L. Su, J. Power Sources 186 (2009) 194–200.
[20] Y.N. Wu, S.J. Liao, Acta Phys. Chim. Sin 26 (2010) 669–674.
[21] Y.N. Wu, S.J. Liao, Z.X. Liang, L.J. Yang, R.F. Wang, J. Power Sources 194 (2009) 805–810.
[22] C.J. Corcoran, H. Tavassol, M.A. Rigsby, P.S. Bagus, A. Wieckowski, J. Power Sources 195 (2010) 7856–7879.
[23] R. Chetty, S. Kundu, W. Xia, M. Bron, W. Schuhmann, V. Chirila, W. Brandl, T. Reinecke, M. Muhler, Electrochim. Acta 54 (2009) 4208–4215.
[24] K.W. Park, Y.E. Sung, S. Han, Y. Yun, T. Hyeon, J. Phys. Chem. B 108 (2003) 939–944.
[25] J. Luo, L. Wang, D. Mott, P.N. Njoki, Y. Lin, T. He, Z. Xu, B.N. Wanjana, I.I.S. Lim, C.-J. Zhong, Adv. Mater. 20 (2008) 4342–4347.
[26] X.X. Wang, J.N. Wang, L.F. Su, J. Power Sources 186 (2009) 194–200.
[27] J. Prabhuram, R. Manoharan, J. Power Sources 74 (1998) 54–61.
[28] Z. Jusys, J. Kaiser, R.J. Behm, Langmuir 19 (2003) 6759–6769.
[29] B. Beden, F. Hahn, J.M. Léger, C. Lamy, C.L. Perdriel, N.R. De Tacconi, R.O. Lezna, A.J. Arvia, J. Electroanal. Chem. Interfacial Electrochem. 301 (1991) 129–138.
[30] H. Wang, C. Xu, F. Cheng, M. Zhang, S. Wang, S.P. Jiang, Electrochem. Commun. 10 (2008) 1575–1578.
[31] C.C. Chen, C.S.C. Bose, K. Rajeshwar, J. Electroanal. Chem. 350 (1993) 161–176.
[32] W. Chen, J. Kim, S. Sun, S. Chen, J. Phys. Chem. C 112 (2008) 3891–3898.
[33] J. Zeng, S. Liao, J.Y. Lee, Z. Liang, Int. J. Hydrogen Energy 35 (2010) 942–948.
[34] H. Ye, R.M. Crooks, J. Am. Chem. Soc. 129 (2007) 3627–3633.